CHAPTER SEVENTEEN

Imaging Changes in the Cytosolic ATP-to-ADP Ratio

Mathew Tantama*, Gary Yellen†,1

*Department of Chemistry, Purdue University, West Lafayette, Indiana, USA
†Department of Neurobiology, Harvard Medical School, Boston, Massachusetts, USA
[1]Corresponding author: e-mail address: gary_yellen@hms.harvard.edu

Contents

Abstract

Adenosine triphosphate (ATP) is a central metabolite that plays fundamental roles as an energy transfer molecule, a phosphate donor, and a signaling molecule inside the cells. The phosphoryl group transfer potential of ATP provides a thermodynamic driving force for many metabolic reactions, and phosphorylation of both small metabolites and large proteins can serve as a regulatory modification. In the process of phosphoryl transfer from ATP, the diphosphate ADP is produced, and as a result, the ATP-to-ADP ratio is an important physiological control parameter. The ATP-to-ADP ratio is directly proportional to cellular energy charge and phosphorylation potential. Furthermore, several ATP-dependent enzymes and signaling proteins are regulated by ADP, and their activation profiles are a function of the ATP-to-ADP ratio. Finally, regeneration of ATP from ADP can serve as an important readout of energy metabolism and mitochondrial function. We, therefore, developed a genetically encoded fluorescent biosensor tuned to

Methods in Enzymology, Volume 547
ISSN 0076-6879
http://dx.doi.org/10.1016/B978-0-12-801415-8.00017-5

sense ATP-to-ADP ratios in the physiological range of healthy mammalian cells. Here, we present a protocol for using this biosensor to visualize energy status using live-cell fluorescence microscopy.

1. INTRODUCTION

We have developed genetically encoded fluorescent biosensors for monitoring the ATP-to-ADP ratio (Berg, Hung, & Yellen, 2009; Tantama, Martínez-François, Mongeon, & Yellen, 2013) and the NADH-to-NAD ratio (Hung, Albeck, Tantama, & Yellen, 2011) in live cells. These biosensors can be used to monitor activity-dependent brain energy metabolism in neurons and astrocytes. Here, we provide a protocol for visualizing the ATP-to-ADP ratio in live cells, and we refer to a separate protocol for visualizing the NADH-to-NAD ratio in live cells (Hung & Yellen, 2014).

1.1. Brain energy metabolism

The brain consumes large amounts of energy to support the information processing and transmission that it carries out (Harris, Jolivet, & Attwell, 2012). A fundamental aspect of brain research has therefore been to study how energy is spent in different cell types on the various steps in signaling (Howarth, Gleeson, & Attwell, 2012). Some of these steps include, for example, action potential generation, maintenance of resting potentials, neurotransmitter metabolism, synaptic vesicle transport, and vesicle cycling (Rangaraju, Calloway, & Ryan, 2014; Zala et al., 2013). Conversely, there is also a fundamental need to understand how this large energy demand is met in different cell types and to what extent the metabolic burden imposed by neuronal activity is distributed across both neurons and astrocytes (Bélanger, Allaman, & Magistretti, 2011; Howarth et al., 2012; Ivanov et al., 2014). Asking and answering these questions at the molecular, cellular, and tissue levels provide a basis for improving clinical diagnostic methods such as MRI and PET imaging (Attwell et al., 2010; Raichle & Mintun, 2006) and for understanding metabolic failures in neurodegenerative conditions such as Alzheimer's disease (Bateman et al., 2012).

However, studying energy metabolism with cellular and molecular resolution poses particular challenges in the brain. Brain tissue is complex and heterogeneous in nature, and signaling activity is continuous and dynamic.

This anatomy and physiology calls for methods to interrogate cellular biochemistry with excellent spatial and temporal resolution. Optical imaging is a technique well suited to meet these demands because it enables continuous observation and typically achieves the spatial resolution and structural detail to make cell type and subcellular distinctions. Optical imaging also naturally pairs well with electrophysiology, providing the ability to study activity-dependent changes. Furthermore, optical sensors and labels, in particular genetically encoded fluorescent biosensors, can track specific biochemical parameters (Akerboom et al., 2013; Hou, Vankatachalam, & Cohen, 2014; Marvin et al., 2013; St-Pierre et al., 2014).

In regards to brain energy metabolism, both ATP level and the ATP-to-ADP ratio are central indicators of cellular energy status, which includes mitochondrial bioenergetic function. Genetically encoded biosensors of the ATP level have been developed and used to study neuronal function (Imamura et al., 2009; Mollajew, Toloe, & Mironov, 2013; Rangaraju et al., 2014). A genetically encoded biosensor of the ATP-to-ADP ratio has also been used to study vesicular transport in axons (Berg et al., 2009; Zala et al., 2013). We developed a second-generation biosensor that senses ATP-to-ADP ratios in the physiological range of healthy mammalian cells (Tantama et al., 2013), and here we provide a protocol for ratiometric fluorescence imaging of this biosensor, called PercevalHR, expressed in live cells.

1.2. Design of PercevalHR, a biosensor of ATP-to-ADP ratio

The PercevalHR biosensor (Tantama et al., 2013) is a single gene product that contains two domains, a sensing domain and reporting domain. These two domains are physically coupled such that MgATP binding causes a conformational change in the sensing domain that is transduced into a conformational change in the reporting domain. The transduced perturbation causes a change in the optical signal provided by the reporting domain, which can be monitored with microscopy.

The sensing domain is based on a MgATP-binding protein, GlnK, from the extremophile *Methanococcus jannaschii* (Berg et al., 2009; Fig. 17.1). GlnK is a homotrimer, but in PercevalHR the subunits are fused in tandem using peptide linkers. As a homotrimer, GlnK also has three MgATP-binding sites that are characterized by a peptide loop, called the T-loop. It is the T-loop that undergoes a major conformational change when MgATP binds. In

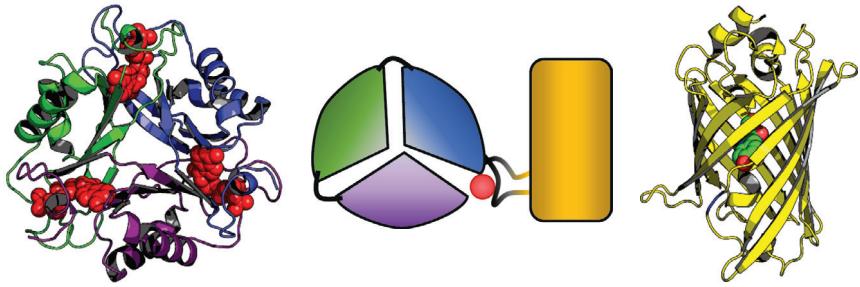

Figure 17.1 Design of PercevalHR. Left, the MgATP-binding protein GlnK (PDB 2J9C) is a homotrimer. Monomers are colored (purple, green, blue), and MgATP spheres are shown in red. Right, the yellow fluorescent protein Venus (PDB 1MYW). Center, a diagram of PercevalHR, a single gene product in which GlnK has been fused to a circularly permuted version of Venus. When MgATP (red) binds, the conformational change in GlnK is transduced to Venus, altering its fluorescence.

PercevalHR, the fused-in-tandem GlnK protein is modified by deleting two of the T-loops, leaving one intact MgATP-binding site.

The reporting domain is the yellow fluorescent protein, monomeric Venus (Nagai et al., 2002). The Venus protein was modified through circular permutation, which serves to move the N- and C-termini to positions in closer physical proximity to the interior chromophore (Nagai, Sawano, Park, & Miyawaki, 2001), creating a variant called cpmVenus. In order to couple the two domains, short peptide linkers were used to insert the cpmVenus as a fusion within the single remaining T-loop of the sensing domain (Fig. 17.1). Thus, when MgATP binds PercevalHR, the T-loop movement perturbs the local environment around the cpmVenus chromophore, resulting in a spectral change in its fluorescence.

1.3. PercevalHR principle of operation

PercevalHR is "ratiometric" in two ways: it senses the ATP-to-ADP ratio, and it exhibits a fluorescence signal that can be measured as a spectral ratio.

How does PercevalHR sense the ATP-to-ADP ratio as opposed to sensing the absolute concentration of ATP? PercevalHR can bind both MgATP and ADP with very high affinity ($K_{1/2} \sim 1\ \mu M$). In the cytosol, the concentrations of ADP and MgATP range in the hundreds of micromolar and several millimolar, respectively. Thus, when PercevalHR is expressed inside cells, its binding site is effectively always occupied by ADP or MgATP.

As a result, there is competition for binding between these two ligands, and PercevalHR senses the ratio of MgATP to ADP because the fluorescence spectrum of the MgATP-bound biosensor is different from that of the ADP-bound biosensor. Furthermore, the nucleotide association and dissociation rates are fast enough to respond to physiological changes in the ATP-to-ADP ratio that occur within seconds.

The difference in fluorescence between the MgATP-bound biosensor and the ADP-bound biosensor is seen in their fluorescence excitation spectra. There are two peaks in the PercevalHR fluorescence excitation spectrum because the cpmVenus chromophore can exist in two charge states. The neutral, protonated chromophore is called the "A-state" and is maximally excited at a peak wavelength of ~420 nm. The anionic, deprotonated chromophore is called the "B-state" and is maximally excited at a peak wavelength of ~500 nm. There is an equilibrium between these two charge states, which is the source of the two peaks in the excitation spectrum for PercevalHR, and ligand binding can shift the equilibrium. The protein conformation when MgATP is bound favors the B-state, whereas the ADP-bound conformation favors the A-state. Hence, the spectral ratio between fluorescence emission intensities measured when PercevalHR is excited at 500 nm versus when it is excited at 420 nm reports the ATP-to-ADP ratio (Fig. 17.2).

In addition to reporting the ATP-to-ADP ratio, measuring the spectral ratio is advantageous for quantitative live-cell imaging. For a sensor that is not spectrally ratiometric, a single fluorescence intensity is the only readout. However, fluorescence intensity is proportional to the number of sensor molecules excited. When comparing two different cells or compartments, it then becomes unclear whether a difference in fluorescence intensity is due to a real metabolic difference or an artifact of different expression levels. This problem can be compounded in time series measurements, where it is also unclear if a decrease in fluorescence intensity is due to metabolic changes or an artifact of photobleaching. These problems are circumvented for spectrally ratiometric sensors because the spectral ratio intrinsically normalizes for the amount of biosensor.

In contrast to PercevalHR's fluorescence excitation spectra, the shape of the fluorescence emission spectra from the two bound states is not significantly different. The biosensor always exhibits green fluorescence emission at a peak wavelength of ~510 nm because of excited-state proton transfer that occurs when the A-state is excited (Hanson et al., 2002; McAnaney, Park, Hanson, Remington, & Boxer, 2002).

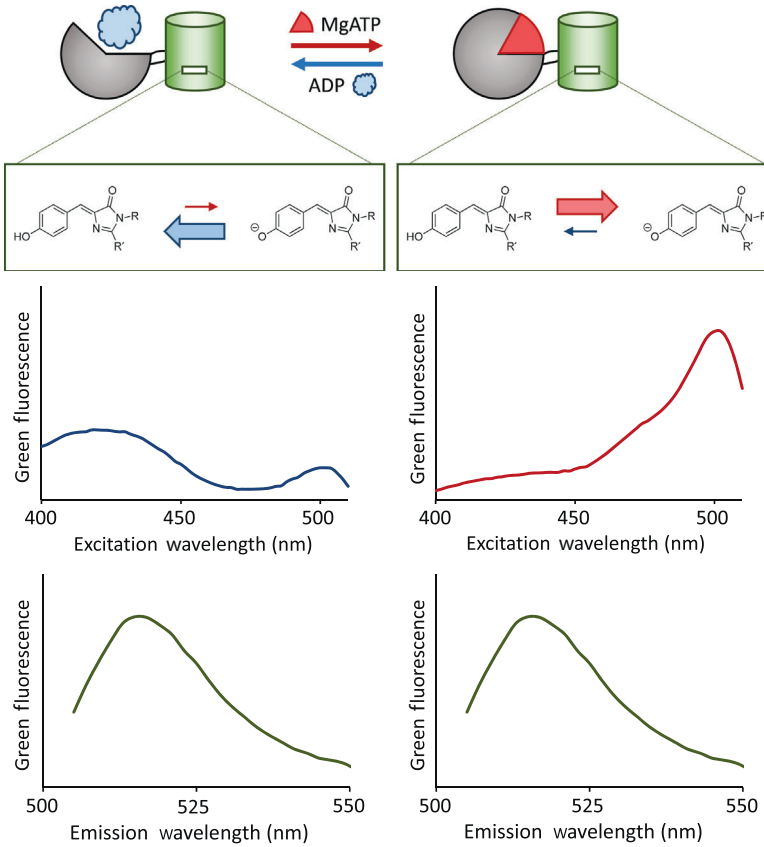

Figure 17.2 Ligand-dependent PercevalHR fluorescence. ADP (blue; light gray cloud in print version) bound to the GlnK domain (gray partial circle) shifts the Venus (green; light gray cylinder in print version) chromophore charge state equilibrium (box), favoring the neutral protonated A-state. MgATP (red; dark gray in print version) binding favors the anionic deprotonated B-state. Ligand binding affects the shape of the fluorescence excitation spectrum (middle). The shape of the fluorescence emission spectrum is not significantly different between states (bottom).

1.4. pHRed

PercevalHR is pH sensitive. This can be a problem when using the biosensor in live cells because cytosolic pH can differ between cells or over time in the same cell. A direct solution to this problem is to make a simultaneous measurement of pH in the same cell expressing PercevalHR. To do this, we also developed a genetically encoded red fluorescent pH biosensor called pHRed (Tantama, Hung, & Yellen, 2011). pHRed is spectrally compatible with PercevalHR, and it is also spectrally ratiometric itself. Thus, for live-cell

imaging experiments, PercevalHR and pHRed were coexpressed and simultaneously imaged.

2. METHODS

2.1. Fluorescent biosensor constructs

PercevalHR and pHRed constructs are distributed through Addgene. Gene expression in mammalian cells was driven by either the cytomegalovirus promoter or human ubiquitin C promoter.

2.2. Expression of biosensors in cultured cells

We have coexpressed PercevalHR and pHRed in a number of cell types including human embryonic kidney cells (HEK293), mouse neuroblastoma cells (Neuro2A), and cultured dissociated mouse hippocampal neurons.

HEK293 cells (ATCC CRL-1573) and Neuro2A cells (ATCC CCL-131) were cultured at 37 °C in a humidified incubator with a 95% air and 5% CO_2 atmosphere. Cells were grown in Dulbecco's Modified Eagle Medium supplemented with 10% fetal bovine serum. Note, we have used several variations of the media formulation (e.g., low glucose, high glucose, glutamine supplemented, GlutaMAX supplemented) without significant differences. Cells were passaged every 2–3 days before reaching greater than 80% confluency. For imaging experiments, cells were seeded onto #1.5 glass coverslips. Coverslips were submerged and coated in a 1 mg/mL solution of protamine (sulfate salt from salmon sperm) in phosphate-buffered saline (PBS) for at least 30 min at room temperature. Coverslips were washed three times with PBS before seeding cells at 40% confluency. Cells were allowed to attach to the coverslip for 6–8 h before transfection. Cells were transfected using Effectene Transfection Reagent (Qiagen) according to the manufacturer's instructions. Cells were incubated with transfection complex for 8–16 h, and then the media was changed.

Mouse embryonic hippocampal neurons were cultured at 37 °C in a humidified incubator with a 95% air and 5% CO_2 atmosphere. Neurons were grown in Neurobasal media supplemented with B-27 supplement, 2 m*M* GlutaMAX, 100 U/mL penicillin, and 100 μg/mL streptomycin (Invitrogen). Neurons were plated on #1.5 glass coverslips. Glass coverslips were cleaned in concentrated nitric acid (~70%) for 24 h, washed extensively with water over 24–72 h with multiple water changes, and allowed to dry for storage in a sterile biosafety cabinet under ultraviolet light. Before

use, coverslips were submerged and coated in a solution of 0.1 mg/mL poly-lysine in PBS overnight at 37 °C. Immediately before seeding neurons, coating solution was removed, coverslips were washed three times with PBS, and rinsed twice with neuron growth media.

Primary cultures of hippocampal neurons were made from 16-day-old to 18-day-old mouse embryos harvested from a euthanized pregnant mouse (Giménez-Cassina et al., 2012). Embryos were rinsed and collected in ice-cold Hank's Balanced Salt Solution (HBSS) supplemented with 1.26 m*M* $CaCl_2$, 0.49 m*M* $MgCl_2$, and 0.40 m*M* $MgSO_4$. Embryos were decapitated, and hippocampal tissue was dissected in HBSS containing Ca^{2+} and Mg^{2+}. Then, the tissue was cut into small pieces, collected, and rinsed in divalent-free HBSS. A solution of 0.25% trypsin and 1 mg/mL DNase I in divalent-free HBSS was added, and the tissue was incubated in a 37 °C water bath with gentle agitation every 5 min. The tissue was allowed to settle by gravity for 30 s, and trypsin solution was removed. The tissue was rinsed twice with warm HBSS and rinsed once with warm neuron media. Fresh media was added, and the tissue was mechanically dissociated with flame-polished glass Pasteur pipettes by manual trituration for 25–50 gentle passages through the pipette. Dissociated cells were passed through a 40-μm cell strainer to remove any remaining large tissue debris. Live-cell counts were obtained using Trypan Blue, and neurons were plated on glass coverslips at densities ranging from 50,000 to 500,000 cells/cm^2. Neurons were allowed to attach for 4 h, and then gently rinsed three times with fresh warm neuron media to remove excess debris. Fresh media or media containing lentivirus was then added typically at a surface area to volume ratio of 0.26 mL/cm^2 growth area. Every 2–3 days 35% of the media volume was replenished with fresh neuron media. We did not regularly use cytosine arabinofuranoside (ara-C) or other antimitotic agents. Glial growth was not a problem, and neuron health was anecdotally more variable in the presence of ara-C as assessed by morphology and fasciculation.

Cultured neurons were typically transduced after 0–1 days *in vitro* (DIV). Lentivirus particles (Massachusetts General Hospital Viral Vector Core) were pseudotyped with Vesicular Stomatitis Virus Glycoprotein. Viral supernatants at titers of $\sim 10^6$ to $\sim 10^8$ infectious units per milliliter (IU/mL) without concentration were stored at −80 °C until use. Neurons were allowed to attach on the glass coverslip for 4–24 h. Half the media was removed and kept sterile for refeeding, and neurons were transduced with an equal volume of fresh neuron media containing lentivirus supplemented with 100 μ*M* D-2-amino-5-phosphonovalerate (APV) to reduce

excitotoxicity due to the viral supernatant (OptiMEM). Lentivirus was added at a multiplicity of infection between 1 and 5 IU/cell. Neurons were incubated with lentivirus for 4–24 h, after which neurons were gently rinsed three times with warm neuron media, and a 1:1 volume mixture of the conditioned media and fresh media was added. Astrocyte-conditioned media can be used for wash and refeeding steps to improve survival.

2.3. Live-cell imaging of fluorescent biosensors

Widefield fluorescence live-cell microscopy was performed on a Nikon TiE inverted microscope equipped with a Nikon Perfect Focus System, a Prior Scientific motorized stage, an Andor Revolution Differential Spinning Disk (DSD) structured illumination system, and controlled using Andor iQ software. Excitation light was provided by a Lumencor Spectra X LED Light Engine coupled with a 1-mm silica fiber light guide. An Andor Clara interline CCD camera was used for detection. A Nikon Plan Apo VC 20X (0.75 NA) dry objective was used for imaging.

Fluorescence imaging of cells coexpressing PercevalHR and pHRed was performed with four excitation and emission combinations (channels). Filter configurations for each channel are summarized in Table 17.1. A dual-band Chroma 59022bs dichroic was used to separate excitation and emission light

Table 17.1 Channel filter configurations

	Lumencor spectra X source		**Andor revolution DSD system**			
	LED channel	**Excitation filter**	**Excitation filter**	**Dichroic**	**Emission filter**	**Camera blocking filter**
Channel 1 PercevalHR B-Band	Cyan	Semrock FF01-482/25	Omega 490HSP	Chroma 59022bs	Semrock FF01-525/39	Chroma 59022m
Channel 2 PercevalHR A-Band	Blue	Semrock FF01-438/24	Omega 490HSP	Chroma 59022bs	Semrock FF01-525/39	Chroma 59022m
Channel 3 pHRed B-Band	Yellow	Semrock FF01-575/25	Omega 590HSP	Chroma 59022bs	Semrock FF01-629/56	Chroma 59022m
Channel 4 pHRed A-Band	Blue	Semrock FF01-438/24	Omega 590HSP	Chroma 59022bs	Semrock FF01-629/56	Chroma 59022m

in the DSD unit for both biosensors. For PercevalHR, green fluorescence emission was collected using a 525/39 nm bandpass filter in the DSD emission filter position. B-band fluorescence was excited using a 482/25 nm bandpass filter in the Lumencor source (Channel 1). A-band fluorescence was excited using a 438/24 nm bandpass filter in the Lumencor source (Channel 2). A 490-nm shortpass filter in the DSD excitation filter position was used for secondary clean-up of excitation and emission light. For pHRed, red fluorescence emission was collected using a 629/56 nm bandpass filter in the DSD emission filter position. B-band fluorescence was excited using a 575/25 nm bandpass filter in the Lumencor source (Channel 3). A-band fluorescence was excited using a 438/24 nm bandpass filter in the Lumencor source (Channel 4). A 590-nm shortpass filter in the DSD excitation filter position was used for secondary clean-up of excitation and emission light. A final dual-band Chroma 59022 m blocking filter was used after the DSD unit and before the camera. Exposure times of 25–200 ms were typical at 2×2 or 4×4 pixel binning. Four channel image sets were typically taken every 15 s for time series experiments, with no delay between individual channel acquisitions.

Cells were imaged with continuous perfusion of heated imaging solution. Imaging solution was an artificial cerebrospinal fluid (ACSF: 10 m*M* HEPES buffer, pH 7.4, 25 m*M* $NaHCO_3$, 120 m*M* NaCl, 2.5 m*M* KCl, 1.25 m*M* NaH_2PO_4, 2 m*M* $CaCl_2$, 1 m*M* $MgCl_2$) continuously bubbled with 5% CO_2 balanced with 95% air or balanced with 95% oxygen. Imaging solution was typically supplemented with 10 m*M* glucose. Imaging solution was warmed to 32–34 °C using an inline heater (Warner) placed immediately before the imaging chamber. A custom imaging chamber was built to accept 18-mm #1.5 glass coverslips such that the coverslip with attached cells served as the chamber floor. House vacuum was used for bath perfusion outflow.

2.4. Ratiometric image analysis

Ratiometric image analysis was performed in ImageJ. Background images of a clean glass coverslip were taken with the same image acquisition parameters used for each channel, each field of view, and each experiment. Field illumination was typically even, and spectral crosstalk was negligible, as determined in control and individual biosensor expression experiments. Background images were subtracted from the raw images in the time series for each respective channel. The mean and standard deviation pixel

intensities were also measured for each of the four channel-background images. A pixel was considered above background if its background-subtracted intensity was greater than or equal to three times the measured background standard deviation. This threshold was used to create a mask and remove (set to zero value) background pixels. Ratio images for PercevalHR were obtained from pixel-by-pixel division of Channel 1 images by Channel 2 images (Fig. 17.3). Ratio images for pHRed were obtained from pixel-by-pixel division of Channel 3 images by Channel 4 images. A region of interest was then drawn around a whole cell or subcellular area to obtain a mean ratiometric signal. Note that pixel-by-pixel division can require image alignment between channels and compensation for chromatic aberration of the microscope system, particularly with any type of optical sectioning techniques.

2.5. Calibration to reduce pH artifacts

To minimize pH artifacts in the PercevalHR signal, a calibration was performed either in the PercevalHR ATP-saturated (ceiling) or ADP-saturated (floor) state. The ATP-saturated state was obtained at the beginning of the experiment after equilibration in the imaging solution which contains excess glucose. The ADP-saturated state was obtained at the end of the experiment by adding the glycolytic poison iodoacetic acid (0.5–1 m*M*), the mitochondrial poisons oligomycin or rotenone (0.5–2.5 μ*M*), or a combination of

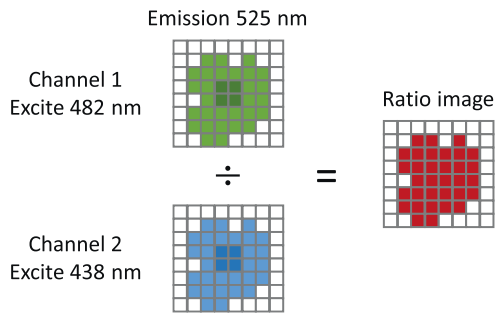

Figure 17.3 Ratiometric image analysis of a cell expressing PercevalHR. Pixelated cartoons of fluorescence images of a cell (left). Images from Channels 1 (top, green) and 2 (bottom, blue) show uneven distribution of the fluorescence intensity. This could be due to cell structure (e.g., nucleus) or a true difference in ATP-to-ADP ratio. The fluorescence intensity images alone cannot distinguish the two possibilities. Pixel-by-pixel division of the Channel 1 image by the Channel 2 image results in the Ratio image (right, red). The ratio image is normalized for biosensor concentration, revealing a homogeneous signal and ATP-to-ADP ratio throughout the cell.

poisons. During the ceiling or floor state, the NH_4Cl "pre-pulse" method was used to induce a transient alkalinization followed by transient acidification of the cytosol. This was induced with a 2–5 min application of 5–15 m*M* NH_4Cl in imaging solution (Roos & Boron, 1981). In solution, NH_4^+ is in acid–base equilibrium with dissolved NH_3, which can diffuse across the plasma membrane into the cell. When NH_3 diffuses into the cytosol, it likewise equilibrates with NH_4^+, and thus NH_4Cl initially causes the cytosol to alkalinize. When extracellular NH_4Cl is removed, equilibration causes the reverse process to occur, and thus the cytosol acidifies. When using the NH_4Cl pre-pulse method, the minimum NH_4Cl concentration and duration of application is used to minimize energy consumption.

The data points from the PercevalHR and pHRed fluorescence ratio signals measured during the NH_4Cl pre-pulse are used to "normalize" and remove pH artifacts from the entire experimental time course. An empirical linear correlation of the PercevalHR signal versus the pHRed signal is measured. The linear relationship is used to transform the pHRed signal to a scaled estimate of the changes in the PercevalHR signal due solely to pH fluctuations over the entire experimental time course. The PercevalHR signal is then divided by the transformed pHRed signal to remove pH artifacts. This "pH-corrected" signal can be further transformed into a biosensor occupancy using the measured fluorescence signals during the ceiling and floor states to scale the maximum observed dynamic range in the cell being analyzed. The occupancy provides an estimated range of ATP-to-ADP ratios.

3. EXPECTED RESULTS

3.1. Biosensor expression

We were able to coexpress PercevalHR and pHRed in several different types of mammalian cells, including primary neurons (Fig. 17.4). The time

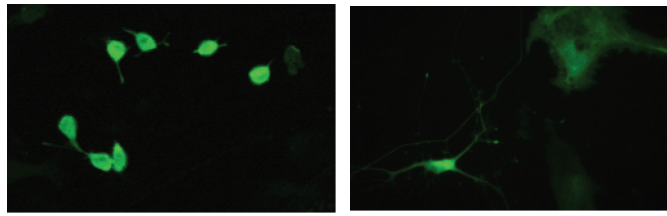

Figure 17.4 PercevalHR expression in the cytosol of Neuro2A cells (left) and in a sparse coculture of neurons and astrocytes (right).

course for appearance of biosensor fluorescence varied depending on the viral or mammalian promoter that was used to drive gene expression. Typically, we waited 2–3 days before reasonable fluorescence signals could be measured, indicating either slower or weaker expression compared to a typical EGFP expression time course. We also have noticed punctate accumulation of pHRed in acidic compartments, putatively thought to be lysosomes (Katayama, Kogure, Mizushima, Yoshimori, & Miyawaki, 2011; Katayama, Yamamoto, Mizushima, Yoshimori, & Miyawaki, 2008), after long expression times that depend on the cell type (typically after 1 week). The ratiometric dye SNARF-5F (Invitrogen) is also spectrally compatible with PercevalHR and can be used as an alternative to pHRed (Berg et al., 2009).

3.2. Metabolic poisoning and performance of the pH calibration

PercevalHR is pH sensitive like many fluorescent sensors, both genetically encoded and small molecule. Without some type of pH correction, misinterpretation of signal changes can easily occur. For example, a pure decrease in pH would cause a signal change that imitates and could be misinterpreted as a reduction in the ATP-to-ADP ratio. To correct for pH artifacts, we developed a protocol that can be carried out in every experiment and on a cell-by-cell basis. This protocol utilizes the NH_4Cl pre-pulse method which has been used extensively to transiently alter and study intracellular pH (Roos & Boron, 1981). The NH_4Cl pre-pulse is applied while the cell has excess fuel to maintain a high energy state and PercevalHR is ATP-saturated, or it is applied while the cell is metabolically inhibited and PercevalHR is ADP-saturated. By these means, the ATP-to-ADP ratio is clamped, and the signal change induced by the NH_4Cl pre-pulse is due solely to the changing pH, revealing PercevalHR's pH sensitivity as measured it in the intracellular milieu.

To demonstrate how this pH calibration performs, we coexpressed PercevalHR and pHRed in HEK293 cells. The cells were imaged in a bathing solution containing 20 m*M* glucose. While clamped in this well-fed, high energy state, the cells were exposed to a short pulse of 5 m*M* NH_4Cl and then 15 m*M* NH_4Cl. Subsequently, 1 m*M* iodoacetic acid was used to block glycolysis and cause a complete depletion of energy stores. As the ATP-to-ADP ratio was decreasing, cells were exposed to a short pulse of 5 m*M* NH_4Cl. Then, when energy stores were completely depleted, cells were exposed to a short pulse of 15 m*M* NH_4Cl. All four NH_4Cl pulses caused the expected changes in PercevalHR and pHRed signals. Metabolic

inhibition with iodoacetic acid also caused acidification of the cytosol. Thus, a pH correction was made using the data points measured during the 15 m*M* NH_4Cl pulse at the beginning (top) or end (bottom) of the experiments. Corrected data using either the top or bottom calibration were indistinguishable, demonstrating the robustness of this protocol. With the pH-corrected PercevalHR signal, it is unambiguous that metabolic poisoning by iodoacetic acid caused a slow decrease in ATP-to-ADP ratio (Fig. 17.5). Thus, a single application NH_4Cl is necessary and sufficient for pH calibration. This NH_4Cl pre-pulse can be applied at the beginning

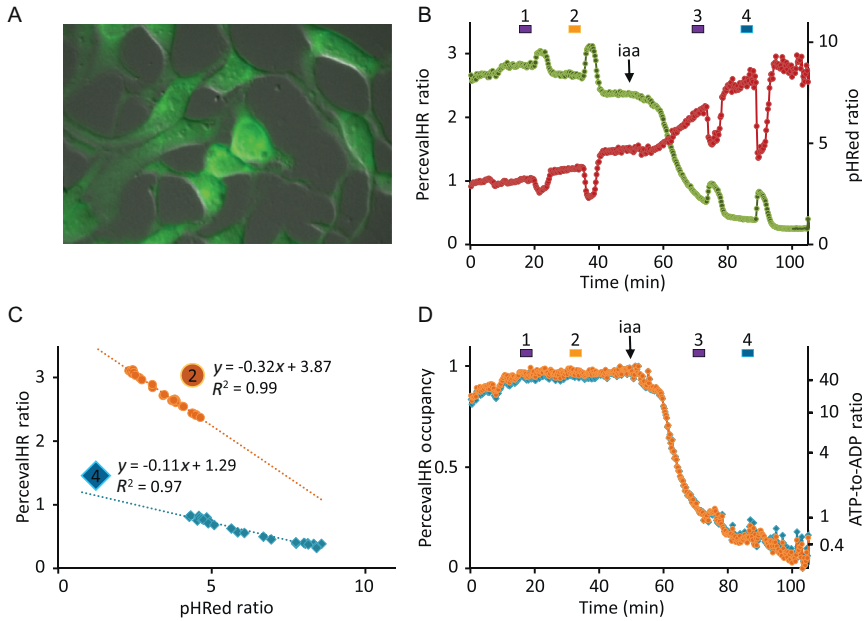

Figure 17.5 Metabolic poisoning and performance of the pH calibration in HEK293 cells coexpressing PercevalHR and pHRed. (A) Green fluorescence overlay on a DIC image of cells. (B) Experimental time course. Left *y*-axis, green data: PercevalHR fluorescence ratio. Right *y*-axis, red data: pHRed fluorescence ratio. Note that pH varies inversely with pHRed ratio. Top bars indicate applications of NH_4Cl at (1) and (3) 5 m*M* and (2) and (4) 15 m*M* for approximately 4 min. Arrow indicates application of 1 m*M* iodoacetic acid (iaa). Cells were imaged in ACSF containing 20 m*M* glucose. Dead time for perfusion was ~2 min. (C) PercevalHR ratio versus pHRed ratio pH calibration curves from NH_4Cl prepulses in the (2) ATP-loaded state (orange, circles) and (4) ADP-loaded state (blue, diamonds). (D) PercevalHR occupancy shows that iodoacetic acid caused a slow reduction in ATP-to-ADP ratio as expected. pH correction using calibration data from the (2) ATP-loaded state (orange, circles) versus (4) ADP-loaded state (blue, diamonds) are not significantly different.

or end of an experiment as convenient, so long as the cell is clamped in a high energy or low energy state during the calibration period.

4. SUMMARY

In conclusion, PercevalHR and pHRed are genetically encoded fluorescent biosensors that can be used to measure and visualize the bioenergetic status of live cells. PercevalHR senses the ATP-to-ADP ratio while pHRed senses pH, and using these biosensors together enables the ATP-to-ADP ratio to be measured free of pH artifacts. In addition, there are a number of other biosensors that have been developed to sense metabolites such as glucose, lactate, pyruvate, and NADH (Hung et al., 2011; Hung & Yellen, 2014; San Martín et al., 2013, 2014; Takanaga, Chaudhuri, & Frommer, 2008; Zhao et al., 2011), and many biosensors can be used to monitor mitochondrial physiology (De Michele, Carimi, & Frommer, 2014). Furthermore, these fluorescent biosensors are versatile and can be used with multiple modes of imaging, including lifetime imaging (Chen, Saulnier, Yellen, & Sabatini, 2014; Tantama et al., 2011, 2013). Thus, using these optical tools in combination with live-cell microscopy and electrophysiology provides powerful method to study activity-dependent brain energy metabolism at the cellular level.

REFERENCES

Akerboom, J., Calderón, N. C., Tian, L., Wabnig, S., Prigge, M., Tolö, J., et al. (2013). Genetically encoded calcium indicators for multi-color neural activity imaging and combination with optogenetics. *Frontiers in Molecular Neuroscience*, *6*, 2.

Attwell, D., Buchan, A. M., Charpak, S., Lauritzen, M., MacVicar, B. A., & Newman, E. A. (2010). Glial and neuronal control of brain blood flow. *Nature*, *468*, 232–243.

Bateman, R. J., Xiong, C., Benzinger, M. D., Fagan, A. M., Goate, A., Fox, N. C., et al. (2012). Clinical and biomarker changes in dominantly inherited Alzheimer's disease. *New England Journal of Medicine*, *367*, 795–804.

Bélanger, M., Allaman, I., & Magistretti, P. J. (2011). Brain energy metabolism: Focus on astrocyte-neuron metabolic cooperation. *Cell Metabolism*, *14*, 724–738.

Berg, J., Hung, Y. P., & Yellen, G. (2009). A genetically encoded fluorescent reporter of ATP:ADP ratio. *Nature Methods*, *6*, 161–166.

Chen, Y., Saulnier, J. L., Yellen, G., & Sabatini, B. L. (2014). A PKA activity sensor for quantitative analysis of endogenous GPCR signaling via 2-photon FRET-FLIM imaging. *Frontiers in Pharmacology*, *5*, 56.

De Michele, R., Carimi, F., & Frommer, W. B. (2014). Mitochondrial biosensors. *The International Journal of Biochemistry & Cell Biology*, *48*, 39–44.

Giménez-Cassina, A., Martínez-François, J. R., Fisher, J. K., Szlyk, B., Polak, K., Wiwczar, J., et al. (2012). BAD-dependent regulation of fuel metabolism and K_{ATP} channel activity confers resistance to epileptic seizures. *Neuron*, *74*, 719–730.

Hanson, G. T., McAnaney, T. B., Park, E. S., Rendell, M. E. P., Yarbrough, D. K., Chu, S., et al. (2002). Green fluorescent protein variants as ratiometric dual emission pH sensors. 1. Structural characterization and preliminary application. *Biochemistry*, *41*, 15477–15488.

Harris, J. J., Jolivet, R., & Attwell, D. (2012). Synaptic energy use and supply. *Neuron*, *75*, 762–777.

Hou, J. H., Vankatachalam, V., & Cohen, A. E. (2014). Temporal dynamics of microbial rhodopsin fluorescence reports absolute membrane voltage. *Biophysical Journal*, *106*, 639–648.

Howarth, C., Gleeson, P., & Attwell, D. (2012). Updated energy budgets for neural computation in the neocortex and cerebellum. *Journal of Cerebral Blood Flow and Metabolism*, *32*, 1222–1232.

Hung, Y. P., Albeck, J. G., Tantama, M., & Yellen, G. (2011). Imaging cytosolic NADH-NAD(+) redox state with a genetically encoded fluorescent biosensor. *Cell Metabolism*, *14*, 545–554.

Hung, Y. P., & Yellen, G. (2014). Live-cell imaging of cytosolic NADH-NAD + redox state using a genetically-encoded fluorescent biosensor. *Methods in Molecular Biology*, *1071*, 83–95.

Imamura, H., Nhat, K. P. H., Togawa, H., Saito, K., Iino, R., Kato-Yamada, Y., et al. (2009). Visualization of ATP levels inside single living cells with fluorescence resonance energy transfer-based genetically-encoded indicators. *Proceedings of the National Academy of Sciences of the United States of America*, *106*, 15651–15656.

Ivanov, A. I., Malkov, A. E., Waseem, T., Mukhtarov, M., Buldakova, S., Gubkina, O., et al. (2014). Glycolysis and oxidative phosphorylation in neurons and astrocytes during network activity in hippocampal slices. *Journal of Cerebral Blood Flow & Metabolism*, *34*, 397–407.

Katayama, H., Kogure, T., Mizushima, N., Yoshimori, T., & Miyawaki, A. (2011). A sensitive and quantitative technique for detecting autophagic events based on lysosomal delivery. *Chemistry & Biology*, *18*(8), 1042–1052.

Katayama, H., Yamamoto, A., Mizushima, N., Yoshimori, T., & Miyawaki, A. (2008). GFP-like proteins stably accumulate in lysosomes. *Cell Structure and Function*, *33*(1), 1–12.

Marvin, J. S., Borghuis, B. G., Tian, L., Cichon, J., Harnett, M. T., Akerboom, J., et al. (2013). An optimized fluorescent probe for visualizing glutamate neurotransmission. *Nature Methods*, *10*, 162–170.

McAnaney, T. B., Park, E. S., Hanson, G. T., Remington, J., & Boxer, S. G. (2002). Green fluorescent protein variants as ratiometric dual emission pH sensors. 2. Excited-state dynamics. *Biochemistry*, *41*, 15489–15494.

Mollajew, R., Toloe, J., & Mironov, S. L. (2013). Single KATP channel opening in response to stimulation of AMPA/kainite receptors is mediated by Na + accumulation and submembrane ATP and ADP changes. *The Journal of Physiology*, *591*, 2593–2609.

Nagai, T., Ibata, K., Park, E. S., Kubota, M., Mikoshiba, K., & Miyawaki, A. (2002). A variant of yellow fluorescent protein with fast and efficient maturation for cell-biological applications. *Nature Biotechnology*, *20*, 87–90.

Nagai, T., Sawano, A., Park, E. S., & Miyawaki, A. (2001). Circularly permuted green fluorescent proteins engineered to sense Ca^{2+}. *Proceedings of the National Academy of Sciences of the United States of America*, *98*, 3197–3202.

Raichle, M. E., & Mintun, M. A. (2006). Brain work and brain imaging. *Annual Review of Neuroscience*, *29*, 449–476.

Rangaraju, V., Calloway, N., & Ryan, T. A. (2014). Activity-driven local ATP synthesis is required for synaptic function. *Cell*, *156*, 825–835.

Roos, A., & Boron, W. F. (1981). Intracellular pH. *Physiological Reviews*, *61*, 296–434.

San Martín, A., Ceballo, S., Baeza-Lehnert, F., Lerchundi, R., Valdebenito, R., Contreras-Baeza, Y., et al. (2014). Imaging mitochondrial flux in single cells with a FRET sensor for pyruvate. *PLoS One*, *9*, e85780.

San Martín, A., Ceballo, S., Ruminot, I., Lerchundi, R., Frommer, W. B., & Barros, L. F. (2013). A genetically encoded FRET lactate sensor and its use to detect the Warburg effect in single cancer cells. *PLoS One*, *8*, e57712.

St-Pierre, F., Marshall, J. D., Yang, Y., Gong, Y., Schnitzer, M. J., & Lin, M. Z. (2014). High-fidelity optical reporting of neuronal electrical activity with an ultrafast fluorescent voltage sensor. *Nature Neuroscience*, *17*, 884–889.

Takanaga, H., Chaudhuri, B., & Frommer, W. B. (2008). GLUT1 and GLUT9 as major contributors to glucose influx in HepG2 cells identified by a high sensitivity intramolecular FRET glucose sensor. *Biochimica et Biophysica Acta*, *1778*, 1091–1099.

Tantama, M., Hung, Y. P., & Yellen, G. (2011). Imaging intracellular pH in live cells with a genetically-encoded red fluorescent protein sensor. *Journal of the American Chemical Society*, *133*, 10034–10037.

Tantama, M., Martínez-François, J. R., Mongeon, R., & Yellen, G. (2013). Imaging energy status in live cells with a fluorescent biosensor of the intracellular ATP-to-ADP ratio. *Nature Communications*, *4*, 2550.

Zala, D., Hinckelmann, M.-V., Yu, H., Lyra da Cunha, M. M., Liot, G., Cordeliéres, F. P., et al. (2013). Vesicular glycolysis provides on-board energy for fast axonal transport. *Cell*, *152*, 479–491.

Zhao, Y., Jin, J., Hu, Q., Zhou, H.-M., Yi, J., Yu, Z., et al. (2011). Genetically encoded fluorescent sensors for intracellular NADH detection. *Cell Metabolism*, *14*, 555–566.